HHS Public Access

Author manuscript

ACS Nano. Author manuscript; available in PMC 2020 November 26.

Published in final edited form as:

ACS Nano. 2019 November 26; 13(11): 12393–12407. doi:10.1021/acsnano.9b05115.

Nanodelivery of mycophenolate mofetil to the organ improves chronic rejection

Mayuko Uehara[1,‡], **Baharak Bahmani**[1,‡], **Liwei Jiang**[1,‡], **Sungwook Jung**[1], **Naima Banouni**[1], **Vivek Kasinath**[1], **Zhabiz Solhjou**[1], **Zhao Jing**[1], **Farideh Ordikhani**[1], **Munhyung Bae**[2], **Jon Clardy**[2], **Nasim Annabi**[3], **Martina M. McGrath**[1,*], **Reza Abdi**[1,*]

[1]Transplantation Research Center, Renal Division, Brigham and Women's Hospital, Harvard Medical School, Boston, MA, USA

[2]Department of Biological Chemistry and Molecular Pharmacology, Harvard Medical School, Boston, MA, USA

[3]Department of Chemical and Biomolecular Engineering, University of California Los Angeles, Los Angeles, CA, USA

Abstract

Inflammation occurring within the transplanted organ from the time of harvest is an important stimulus of early alloimmune reactivity, and promotes chronic allograft rejection. Chronic immune-mediated injury remains the primary obstacle to the long-term success of organ transplantation. However, organ transplantation represents a rare clinical setting in which the organ is accessible *ex vivo*, providing a unique opportunity to use nanotechnology to directly deliver therapeutics to the graft. This approach facilitates the directed delivery of immunosuppressive agents (ISA) to locally target pathogenic immune responses prior to the transplantation. Here, we have developed a system of direct delivery and sustained release of mycophenolate mofetil (MMF), to treat the donor organ prior to transplantation. Perfusion of a donor mouse heart with MMF-loaded PEG-PLGA nanoparticles (MMF-NP) prior to transplantation abrogated chronic allograft rejection by suppressing intra-graft pro-inflammatory cytokines and chemokines. Our findings demonstrate that *ex vivo* delivery of an ISA to donor organs using a nanocarrier can serve as a clinically feasible approach to reduce chronic allograft rejection.

[*]Address correspondence to: **Reza Abdi, MD**, Transplantation Research Center, Brigham and Women's Hospital, 221 Longwood Ave, Boston MA 02115, USA, Tel: 617-732-5259, Fax: 617-732-5254, rabdi@rics.bwh.harvard.edu; **Martina M. McGrath**, Transplantation Research Center, Brigham and Women's Hospital, 221 Longwood Ave, Boston MA 02115, USA, Tel: 617-732-5259, Fax: 617-732-5254, MMCGRATH8@BWH.HARVARD.EDU.

Author contributions

M.U. performed microsurgery, performed experiments, analyzed and interpreted data, and drafted the manuscript. B.B. synthesized nanoparticles, performed experiments, immunofluorescence staining, analyzed and interpreted data, and drafted the manuscript. L.J performed immunofluorescence staining, qPCR experiments, and analyzed and interpreted data. S.J. designed, synthesized MPA*-NP and performed experiments. V.K. performed experiments and edited the manuscript. N.B. performed experiments and analyzed data. Z.S, Z.J. and F.O. helped experiments. M.B. helped to synthesize MPA*-NP and performed experiments. C.J and N.A. helped and advised study regarding to nanoparticle. M.M. and R.A. designed the study, interpreted data, and critically revised and finalized the manuscript.

[‡]These authors contributed equally to this work.

Data Availability

All data generated or analyzed during this study are available from the corresponding author on reasonable request.

Competing financial interests

The authors declared that they have no competing interests.

Keywords

Nanodelivery; transplant; mycophenolate mofetil (MMF); chronic rejection; selective drug delivery

Introduction:

Solid organ transplantation was pioneered with the first kidney transplant in 1954 and since then, transplantation has become a mainstay of treatment for patients with end-stage organ failure. Over the ensuing decades, the use of increasingly potent immunosuppressive agents (ISAs) has reduced overall rates of acute transplant rejection and improved short-term graft survival. However, long-term transplant outcomes have failed to improve to the same degree[1,2]. Furthermore, ISAs are a significant contributor to post-transplantation complications such as infection, cardiovascular disease, diabetes and malignancy[3-5]. Attempts to minimize ISAs such as cyclosporin and tacrolimus have had mixed success, and are associated with increased risk of acute transplant rejection[3, 6-7].

Inflammatory responses occurring within the allograft early in the post-transplantation period significantly enhance alloimmunity[8-9]. Intra-graft inflammation begins prior to organ procurement, where upregulation of inflammatory cytokines and adhesion molecules within donor organs occurs simultaneously with brain death[10]. This process peaks in the post-anastomosis period, coincident with extensive ischemia-reperfusion injury (IRI). IRI leads to activation of intra-graft antigen presenting cells, including dendritic cells (DCs)[11-12]. DCs activated by intra-graft inflammation in turn promote alloreactive T cell responses, enhancing chronic alloimmune injury[11-13]. Therefore, the development of more effective strategies to control early immune activating events within the organ and improve long-term transplant outcomes remains a major focus of investigation in transplantation.

Notable progress in synthesizing and characterizing nanoscale materials has sparked interest in refining the methods of drug delivery, especially in the field of oncology. Nanotechnology has been used to improve pharmacokinetic profiles, leading to controlled, sustained release of an agent, and delivery of a drug to the site of interest[14-18]. In contrast to most models of systemic disease, transplantation is a unique scenario, in which the affected organ is accessible for intra-organ delivery of therapeutics. Furthermore, as the graft and its draining lymph nodes are the primary sites of alloimmune priming, targeted delivery of nanoparticle-based therapeutics hold significant potential to improve treatment efficacy and reduce the off-target toxicity that plagues the clinical management of transplant recipients. Therefore, organ transplantation represents a singular situation where innovative nanotherapeutic and diagnostic applications could address many of the thorniest clinical challenges.

Mycophenolate mofetil (MMF) blocks inosine monophosphate dehydrogenase and inhibits purine metabolism in lymphocytes, preventing their proliferation. It is one of the most commonly used immunosuppressive agents following transplantation and has an excellent safety profile[19]. We have engineered a nanoparticle carrier of MMF with excellent loading and release capacity. Herein, we tested the hypothesis that pre-perfusion of the donor heart

with MMF-loaded PEG-PLGA nanoparticles (MMF-NP) would reduce early intra-graft inflammation and prevent chronic allograft rejection.

Results:

Uptake of PLGA nanoparticles by HUVEC cells

To assess the effect of perfusion with PEG-PLGA NP (size: 65nm) on endothelial cells, we firstly assessed their uptake by HUVEC cells as a model of endothelium[20-21]. PEG-PLGA nanoparticles labeled with CF-660 dye (CF660-NPs, red fluorescence) were incubated with HUVEC cells for one hour. Lysosomes were stained using LysoTracker® (green) dye, and images were taken by confocal microscopy. CF660-NPs were detected outside of lysosomes and located around the nuclei of HUVEC cells (Figure 1A). Intracellular CF660-NPs were counted by flow cytometry, which confirmed the uptake of CF660-NP by HUVEC cells within one hour of incubation (Figure 1B). To assess if NPs had an effect on HUVEC cell viability, NPs were incubated with HUVEC cells for 48 and 72 hours. FACS analysis of the cells showed even after 72 hours incubation, NPs did not cause any cell death. (Figure 1C).

In vivo perfusion of heart with PEG-PLGA nanoparticles

To study the kinetics of NPs following delivery to the heart, we synthesized PLGA NPs loaded with IR800 CW (IR800-NP). IR800 CW is a near infrared (NIR) fluorophore that offers several key advantages including; increased optimal penetration depth, due to reduced absorption of photons by water and proteins in the tissue, diminished scattering within the NIR spectral band, and enhanced imaging contrast due to the use of an exogenous fluorophore probe in the setting of minimal autofluorescence in NIR spectral bands.

Following anesthesia of the donor mouse, thoracotomy was performed and the heart was perfused with IR800-NP via injection into the inferior vena cava. The heart was then harvested and immersed in UW (University of Wisconsin) solution at 4 °C (Figure 1D), and after 2 hours, was imaged using an iBox® Explorer2 imaging microscope (UVP). The fluorescent signal detected from the entire heart organ demonstrated uniform perfusion of heart tissue with IR800-NP (Figure 1E).

Next, to assess the trafficking of NP following transplantation, a heart perfused with IR800-NP as described above was transplanted into C57BL/6 mouse[22-23]. At day one post-transplantation, IR800 fluorescent signal was detectable from the transplanted heart perfused with IR800-NP, as compared to the heart perfused with PBS (Figure 1F).

Mice were sacrificed at day 1 and day 7 post cardiac transplant and immunofluorescence analysis of the allograft revealed the presence of IR800-NP (red) within the cardiac tissue (green, F-actin) at both time points (Figure 1G). We next examined the distribution of IR800-NPs in vascular and non-vascular compartments of the cardiac allograft. Co-staining with CD31 and CD11b demonstrated that vast majority of IR800-NPs were located within $CD11b^+$ cells (Figure 1H, 1I and 1J).

Synthesis and characterization of MMF-loaded PEG-PLGA NP (MMF-NP)

Mycophenolate mofetil (MMF; Cellcept®) is a prodrug of mycophenolic acid (MPA), and inhibitor of inosine monophosphate dehydrogenase (IMPDH). It is routinely used systemically for prevention of rejection in kidney, liver and heart transplantation[19, 24-26]. We chose MMF to target the organ for pre-treatment, due to its excellent vascular safety profile and lack of end-organ toxicity[27-28]. A mix of polymer and MMF in ethyl acetate was emulsified in the water phase, followed by solvent evaporation and MMF-loaded PEG-PLGA NP (MMF-NP) collection by centrifugation (Figure 2A). The loading efficiency of MMF was calculated as 23±2.7%, which is equal to 39μg of MMF per one dose administration. The average size of our MMF-NP was around 60 nm (Figure 2B), and it was negatively charged (−16.2±0.67) by DLS measurement. Observation under electron microscopy highlighted its round shape, double layer, and size (Figure 2C).

Kinetic of MMF release from MMF-NP *in vitro*

First, we tested for toxicity of MMF-NP on HUVEC cells. MMF-NP were incubated with HUVEC cells for 24, 48 and 72 hours. We did not observe any toxic effects of MMF-NP on HUVEC cells (Figure 2D). Next, the release profile of MMF from MMF-NP was measured *in vitro* under physiological conditions. MMF was released gradually from the NP during the first three days of release test, achieved 60% release by day 7, and the release kinetics remained controlled through Day 10 (Figure 2E).

We then examined the retaining and releasing capacity of MMF from MMF-NP by testing its ability to suppress T cell proliferation *in vitro*. We compared MMF-NP to the same amount of free MMF (39μg). MMF-NP and free MMF suppressed T cell proliferation equally (Figure 2F). To assess the clinical applicability of this approach, we were also interested in examining the retention of MMF following long storage, and test its immunosuppressive capacity. MMF-NP which were stored for 7 and 14 days were washed thoroughly and added to the T cell suppression assay. MMF-NP from both time points showed effective suppression of T cells (Figure 2F), demonstrating the stability of these NP over time.

Biodistribution of labeled MPA by *in vivo* perfusion of heart in transplantation

To observe the distribution of our NP *in vivo*, we wished to use a labeled form of mycophenolic acid (MPA) to generate fluorescent NP. For these experiments, we utilized MPA, instead of its pro-drug MMF, as MPA can be easily conjugated with amine-containing dyes to enable tracking *in vivo*. We labeled MPA (MPA*) directly with amine-functionalized fluorescent dye (amine CF594) and synthesized NP (MPA*-NP).

To assess our ability to detect MPA*-NP in tissue, hearts were perfused either with PBS or MPA*-NP, harvested and immersed in UW solution for 2 hours. The heart perfused with MPA*-NP showed high fluorescent signal in both whole image and cross section image (Figure 3A).

Next, we determined the degree of NP accumulation in the heart allograft when the donor allograft was perfused with NP prior to transplant, as compared to treating the recipient with

systemic administration of NP at the time of transplantation. A group of mice received non-perfused hearts and at the time of transplant, were treated with a similar dose of MPA*-NP by intravenous (IV) injection (recipient systemic IV). These mice were compared with recipients of donor hearts perfused with MPA*-NP at the time of harvest, per usual protocol (donor heart perfusion) (Figure 3B). Six hours after heart transplantation, mice organs were harvested to assess biodistribution of MPA*-NP using fluorescence imaging. The transplanted heart from donor heart perfusion group showed significantly higher fluorescent signal compared to grafts from recipients treated with IV MPA*-NP (Figure 3C). Other organs such as kidney, liver and lung revealed greater accumulation of MPA*-NP, and significantly higher MFI, in recipients treated with systemic IV MPA*-NP, as compared to donor heart perfusion group. (Figure 3D). These data indicate that MPA was delivered to donor heart effectively with perfusion prior to organ transplantation and remained localized, without distribution to other organs in donor heart perfusion group. In contrast, systemic IV injection of MPA*-NP to recipients at the time of transplantation was a less effective method to deliver the active drug to the allograft and led to greater accumulation of NP in peripheral organs.

Suppression of early intra-graft alloimmune response by MMF-NP

Our next objective was to examine the *in vivo* efficacy of MMF-NP in a MHC class II mismatch mouse heart transplant model of chronic allograft rejection. A BM12 mouse heart (donor heart) was perfused with either PBS (control), free MMF, or MMF-NP, then harvested, and immersed in UW solution at 4°C. Two hours later, the heart was transplanted into a C57BL/6 mouse (recipient).

Based on the findings from our previous experiment evaluating the tempo of MMF release from NP (refer Figure 2E), we harvested heart allografts at day 5 post-transplantation. As expected in this model of chronic allograft rejection, there were no differences in cellular infiltration or vascular appearance of the heart grafts on day 5, as assessed by scoring of H&E images the modified ISHLT score (Figure 4A and 4B). However, analysis of heart allografts by qRT-PCR revealed that the allografts perfused with MMF-NP had significantly lower expression of pro-inflammatory cytokines, such as IL-6 and TNFα, in comparison to control and free MMF treated grafts (Figure 4C). Heart allografts perfused with MMF-NP also demonstrated lower expression of other inflammatory cytokines, such as IFNγ, IL-17 and IL-2, but these differences did not reach significance (data not shown). In addition, intra-graft expression of chemokines was also assessed by qRT-PCR. Significant reductions in the expression of CXCL9 was observed in the heart allografts perfused with MMF-NP, as compared to control and free MMF (Figure 4D). Treatment with both MMF-NP and free MMF also led to a significant decrease in expression of CCR5 and CXCR3 as compared to control, although there was no difference seen between the two MMF formulations. (Figure 4D).

On the basis of our findings that MMF-NP suppresses T cell proliferation up to 14 days *in vitro*, we next assessed the status of heart grafts at 14 days post-transplantation. Allografts hearts in all three groups (control, free MMF and MMF-NP) were beating at 14 days post-transplant, when they were harvested for analysis. Histologic assessment revealed moderate

cellular infiltration and vasculopathy in the control group, whereas those perfused with free MMF had mild cellular infiltration and clear vasculature (Figure 4E). Furthermore, heart grafts in the MMF-NP group had little cellular infiltration of the myocytes and clear vasculature (Figure 4E). Consequently, grafts perfused with MMF-NP showed significantly lower scores for cellular infiltration and vascular pathology than control, but comparison with the free MMF group did not reach statistical significance (Figure 4F). On immunofluorescent staining, we also observed fewer $CD3^+$ T cells and $CD11b^+$ cells in heart allografts perfused with MMF-NP, as compared to control and free MMF perfused hearts (Figure 4G).

Pre-transplant donor heart perfusion with MMF-NP abrogates chronic heart rejection

Using this MHC class II mismatch model of chronic rejection, we next performed longer-term observation of the allografts to assess the effect of MMF-NP perfusion at the time of allograft retrieval. At 28 days post-transplant, we harvested the heart allografts, spleens, and draining lymph nodes (DLNs) of recipient mice whose grafts were perfused with either PBS (control), free MMF or MMF-NP prior to transplantation. All allograft hearts were beating at 28 days post-transplant, but the strength of contraction of hearts in the control and free MMF groups were weaker than the MMF-NP treated group. Histologic analysis of the heart allografts in the control group revealed moderate to severe cellular infiltration and occluded vasculature, findings indicative of chronic graft rejection (Figure 5A). In comparison to their appearance at 14 days post-transplantation (refer to Figure 4E, free MMF), by day 28, the heart allografts perfused with free MMF showed progressive graft rejection with moderate cellular infiltration and vasculopathy (Figure 5A). In comparison, allografts perfused with MMF-NP showed much lower cellular infiltration and intact vasculature, consistent with less severe rejection (Figure 5A), and histological appearance was similar to those harvested at day 14 (refer to Figure 4E, MMF-NP). We observed significantly lower scores for both cellular infiltration and vascular appearance in the MMF-NP group in comparison to the control and free MMF groups (Figure 5B), which supported the observations of H&E-stained tissue. The immunofluorescence staining of allograft hearts also showed lower infiltration of $CD3^+$ T cells and $CD11b^+$ cells in MMF-NP group, as compared to the control and free MMF groups (Figure 5C).

Interstitial fibrosis is an important characteristic of chronic allograft rejection[29-30]. The allograft hearts treated with MMF-NP showed significantly less fibronectin staining as compared to control and free MMF groups (Figure 5D). Furthermore, the gene expression of fibronectin in allograft hearts was significantly lower in MMF-NP group (Figure 5E). We also measured the development of donor specific antibody (DSA) to assess chronic alloimmune response. Serum samples collected at day 28 post-transplant were analyzed by FACS to detect DSA-IgG. As shown in Figure 5F, serum collected from MMF-NP group showed significantly less DSA-IgG development compared to other groups. We also evaluated chronic allograft vasculopathy (CAV)[31]. Elastica van Gieson stain of heart allografts harvested on day 28 showed a significant increase of intimal thickness in control and free MMF treated recipients (white arrows). However, the vasculature in those treated with MMF-NP showed less intimal thickening (Figure 5G).

The expression of VCAM, ICAM and P-selectin on endothelium has also been used to assess vasculopathy[31-32]. We next assessed the expression of these genes in allograft hearts, and observed a significant suppression of VCAM and P-selectin expression in the MMF-NP group as compared to control (Figure 5H). To examine the effect of MMF-NP on endothelial cells in greater detail, we also assessed the level of VCAM, ICAM and P-selectin gene expression *in vitro*, using HUVEC cells stimulated with TNFα and incubated with either free MMF or MMF-NP. While, the levels of these genes were very low in untreated HUVEC cells, we noted a marked increase following stimulation with TNFα. This increase was markedly and significantly suppressed by MMF-NP treatment, as compared to control group; and additional suppression was seen over treatment with free MMF alone. (Figure 5I).

Lack of systemic effect of allograft pre-perfusion with MMF-NP despite prolonged local effect on heart allograft

Given the superior histological appearance of the allograft at 28 days post-transplant, we were interested to assess if graft perfusion with MMF-NP prior to transplantation had an effect on peripheral immune responses. Spleens and draining lymph node (DLN) harvested on day 28 post-transplant from mice treated with MMF-NP, free MMF and control (PBS), and were analyzed by flow cytometry. We observed no differences in the frequency of $CD4^+$ and $CD8^+$ T cells in spleen or DLN, between the three groups (Supplementary Figure 1A). Similarly, percentages of $CD4^+CD62L^{low}$, $CD8^+CD62L^{low}$, $CD4^+CD69^+$, $CD8^+CD69^+$ and $CD4^+CD25^+Foxp3^+$ T cells in the spleen and DLN were not statistically different among the three groups (Supplementary Figure 1B).

We then tested the effect of intra-organ delivery on the peripheral alloimmune responses using Elispot and mixed lymphocyte reaction (MLR) of spleen and DLN. In Elispot analysis, we observed no statistically significant differences between groups in spleen and DLN (Supplementary Figure 1C). MLR assay also showed no statistically significant differences between groups in spleen and DLN (Supplementary Figure 1D). These findings suggested that the selective perfusion of heart allografts with MMF-NP suppressed the local intra-graft alloimmune response, but it did not affect the systemic immune response.

Discussion:

Despite significant advances in the care of transplant recipients in recent decades, long-term graft survival remains disappointingly short. Chronic vascular injury, mediated by subclinical alloimmune activation and calcineurin inhibitor toxicity, are important causes of late graft loss[3, 33-34]. The majority of transplanted organs undergo hypothermic perfusion between procurement and transplantation, which provides the opportunity to add therapeutic agents, including nanocarriers, into the preservation fluid. Direct delivery of ISAs to the organ at the time of transplantation could potentiate their efficacy by decreasing intra-graft inflammation and alloimmune activation during this critical period. This approach could also potentially decrease the need for systemic exposure to ISAs, such as calcineurin inhibitors, which have been implicated in microvascular toxicity, accelerated cardiovascular disease, and malignancies[1, 34-39].

Several noteworthy studies have emphasized the importance of intra-graft immune activation in orchestrating allograft rejection[40-41]. Kreisel's group has shown that the alloimmune response underlying acute lung rejection is initiated in the graft itself, and this process is independent of secondary lymphoid tissues[40]. We and others have shown that inflammatory signaling (i.e., ischemia-reperfusion injury) in the graft following transplantation leads to the maturation of allograft-derived dendritic cells and their subsequent trafficking to the host's LN where naive and central memory T cells reside[12-13, 42-48]. Early innate inflammatory responses have been found to be critically regulated by IFNγ-producing endogenous $CD8^+$ T cells present in the recipient before detectable priming of alloantigen T cells[49]. They directly mediate allograft rejection by increasing cytokines such as IL-6 and TNFα, and induce recipient leucocyte (T cells) infiltration into the graft[50]. Similarly, we have recently reported that ischemia leads to increased IL-6 production, increases antigen specific $CD4^+$ T cell graft infiltration is followed by recruitment of IFNγ-producing $CD8^+$ T cells, and results in accelerated rejection[11]. The importance of targeted organ delivery is also highlighted by reports indicating the importance of activated endothelial cells expressing class I and II MHC molecules in addition to the adhesion molecules which directly prime and activate T cells[48, 51-58]. Furthermore, endothelial cells may also play a role in recruiting recipient antigen-presenting cells (APC) to the organ[59-62]. Recent studies have showed the targeting the endothelium by *ex vivo* machine perfusion using NP has been reported in human kidneys which were declined for transplantation[21, 63] and human umbilical vein[20]. Allograft ischemia, which is unavoidable in transplantation, is one of the most significant stimuli to intra-graft inflammation. These studies together exemplify the impact of the intra-graft immune response in the pathogenesis of graft rejection and highlight the importance of engineering therapies aimed at disrupting its development.

In clinical practice, MMF and MPA are routinely and interchangeably used in organ transplantation, due to both efficacy and vascular and metabolic safety profile[19]. We chose MMF for our NP for delivery to the allograft heart, as it has lower polarity than MPA because of the masking of polar carboxylic group, which leads to higher loading efficiency in emulsification, and slower release kinetics from NP, and thereby generating a more effective therapeutic product. MMF, which is a prodrug of MPA, inhibits inosine monophosphate dehydrogenase (IMPDH) interferes with purine synthesis and proliferation of lymphocytes[64-66]. MMF also blocks glycosylation of lymphocyte and monocyte glycoproteins required for adhesion to the endothelial cells, and by reducing the expression of adhesion molecule such as E- and P-selectin, inhibits the leukocyte recruitment into areas of inflammation[67-68]. Early application of MMF to harvested organs, hence, can target alloimmune responses on multiple levels[69]. In addition, MMF is well-tolerated clinically and harbors an excellent vascular safety profile[70]. Similarly to previous reports[20-21, 71], we first assessed the uptake and toxicity of our PEG-PLGA by HUVEC cells. In keeping with findings using with other NPs, these studies also indicated that MMF-NP had no toxic effect on HUVEC cells. We examined the kinetics of release of MMF, which showed a sustained release pattern; and demonstrated the stability of these NP, where both freshly manufactured and stored MMF-NP effectively suppressed T cell proliferation *in vitro*. These data suggest that perfusion of organs prior to transplant not only would suppress immediate events in alloimmune activation, but also could dampen the later phases of chronic rejection as well.

We targeted the donor organ by directly perfusing it with NP, prior to transplantation. Following perfusion of organs with IR800-NP, we assessed the distribution of NP within the organs pre- and post-transplantation. The perfused heart showed a strong signal prior to transplantation and NPs could be distinguished clearly following transplantation, located between the F-actin filaments of the perfused heart, even at 7 days post-transplantation. Perfused NPs were taken up mainly by $CD11b^+$ cells, such as macrophages or monocytes.

One important question was to assess the superiority of NP in delivering drug to the allograft while avoiding peripheral tissue accumulation. To answer this question, we generated NPs with labeled drug and examined the resulting *in vivo* signal, to observe their distribution. For these labeling experiments, we selected MPA over MMF due to technical considerations. Unlike MMF, MPA has a carboxylic acid, which can be easily conjugated with amine-containing dyes by carboxyl-amine crosslinking *via* carbodiimide-mediated coupling chemistry. MPA labeled with amine CF594 (MPA*), was loaded into NP (MPA*-NP), and we examined biodistribution of MPA*-NP *in vivo,* comparing with systemic IV administration into recipient mice. The perfused cardiac allograft showed higher fluorescent signal as the result of higher MPA*-NP levels in the organ than systemic injected cardiac allograft, while the other major organs showed less fluorescent signal in donor heart perfusion group. These results clarified the effectiveness of our localized drug delivery, and emphasized the advantages of this perfusion strategy in terms of avoiding off target effects on other vital organs.

Then, we assessed the efficacy of our MMF-NP in the suppression of chronic allograft rejection *in vivo* at several time points. The mechanism of chronic rejection, an evolving injury that results from repeated alloimmune attacks on the transplant, remains a difficult and unanswered question. We used a model of chronic allograft rejection, an MHC class II mismatch murine heart transplant model, to test the efficacy of MMF-NP in impacting this process. Reflecting the insidious nature of alloimmune injury in chronic rejection, cellular infiltrates or vascular injuries were not prominent at day 5 post-transplantation in any of the treatment groups. Nonetheless, we examined the mRNA transcripts of inflammatory cytokines, as more sensitive markers of early inflammatory responses. Here, we observed significant reduction of expression of pro-inflammatory cytokines, in the allograft hearts perfused with MMF-NP, as compared to the control and free MMF groups. Significant reductions in IL-6 and TNFα and IFNγ were observed, along with reductions in pro-inflammatory chemokines. Among their pro-inflammatory effects, TNFα and IFNγ promote IL-6 expression. IL-6 plays a key role in graft rejection directly by enhancing alloimmune responses and indirectly by augmenting the innate immune response, both of which subsequently enhance graft rejection[72-77]. We have previously shown its central effect in promoting allograft rejection following ischemia reperfusion injury[11]. IL-6 also increases vascular cell adhesion molecule-1 (VCAM-1) and intercellular adhesion molecule-1 (ICAM-1) in the endothelium and thereby facilitates T cell migration to the allograft[78-80]. CXCR3 and its ligand, CXCL9, also play a critical role in the trafficking of pathogenic T cells promoting transplant rejection, including chronic rejection[81]. MMF directly inhibits T lymphocyte proliferation and has been previously demonstrated to decrease expression of adhesion molecules by endothelial cells[67-68]. Our mechanistic data support a role for MMF in decreasing local inflammation within the graft at the time of transplant, and these findings

suggest that decreased lymphocyte trafficking into the transplant may be an important mechanism for the observed improved allograft outcomes.

We next examined allograft hearts at later time points following transplantation histologically. At 14 days, histological evidence of chronic rejection was significantly less advanced in the MMF-NP as compared to the untreated group. We noted a trend toward a protection against chronic rejection in MMF-NP treated as compared to free MMF group. However, by day 28, these differences were more marked. At this time point, both the control and free MMF groups had severe chronic rejection while MMF-NP treated grafts showed a marked reduction in the number of cell infiltrates and vascular injuries. Immune characterization of T cells and macrophages also showed a marked reduction in these cells which play a critical role in the pathogenesis of transplant rejection.

The major characteristics of chronic allograft rejection are fibrosis and allograft vasculopathy[29-31, 82]. The cardiac allograft harvested at 28 days following transplantation showed significantly less fibrosis, low expression of VCAM and P-selectin, and lesser degrees of intimal thickening in MMF-NP treated recipients. Similarly, we found lower levels of DSA in MMF-NP treated recipients. The model of murine heterotopic cardiac transplantation does have some inherent limitations in its ability to examine chronic allograft vasculopathy[31, 83]. However, we observed comprehensive improvements in the assessed measures of chronic allograft rejection in MMF-NP perfused hearts, which we believe resulted from the early decreases in intra-graft inflammation. To more directly examine the effect of MMF-NP on endothelial cell activation, we also returned to the *in vitro* model of TNFα stimulated HUVEC cells, incubated either with PBS, free MMF or MMF-NP and found significant reduction in expression of adhesion molecules after incubation with MMF-NP, similar to our results in the allograft heart.

Given the significant changes we observed in alloimmune activity within the transplant, we next wanted to assess if local delivery of MMF to the organ prior to transplantation, had a modulating effect on peripheral immune responses. By flow cytometry, we assessed the spleen and DLN for frequency of activated $CD4^+$ T cells and $CD8^+$ T cells and Tregs, which showed no difference between three groups. The allospecific response in the periphery was analyzed by Elispot and MLR of spleen and DLN, and we similarly observed no difference between groups, indicating that the impact of MMF-NP on allograft injury was solely mediated by its effects on intra-graft immune activation.

There is currently great interest in the *ex vivo* perfusion of donor organs as a strategy to optimize grafts prior to transplantation[21, 84-86]. The method of static simple cold storage (SCS) is approved for liver grafts, while both SCS and dynamic hypothermic machine perfusion (HMP) are clinically approved for kidneys. The potential to use ISA-loaded nanocarriers (ISA-NP) for targeted drug delivery, has begun to attract considerable attention in the field of transplantation[12, 21-22, 87-88]. Based on the model described here, we speculate that perfusing organs with ISA-NP using currently available perfusion machines could be a readily translatable strategy that could significantly reduce early intra-graft inflammation, decrease alloimmune activation, and thereby improve longer term outcomes. Such findings are supported by previous publications from others[88-89]. By perfusing the donor graft with

ISA-NPs prior to transplantation, the disadvantage of prolonged ischemic time to transplant outcomes could be mitigated.

An interesting future direction will be to investigate the optimal duration of perfusion with NP to maximize ISA delivery to the transplant organ. In our strategy, a one-time perfusion of the allograft, was successful in improving outcomes, and we observed that NP had been taken up into the allograft parenchyma and at later time points were present within $CD11b^+$ antigen presenting cells. Devising the maximally effective strategy to apply this approach will require further evaluation.

Our strategy allows for the delivery of a wide range of combinatorial therapeutics other than ISAs, including drugs ranging from small molecules to antibodies, which underlines its vast potential therapeutic implications. Given the substantial clinical unmet needs in transplantation, we believe that targeted delivery represents a pioneering departure, which could lead to substantial improvements in transplantation outcomes. The FDA has approved the biocompatible and biodegradable PEG-PLGA polymer used in this study for clinical applications, and its routine use in medical materials such as surgical sutures[90-94] demonstrates its excellent safety profile. These data represent an account of the first controlled and targeted formulation of ISA nanomedicine for organ transplantation and this novel approach has significant potential for rapid translation to clinical practice.

In summary, our current study establishes a method of a controlled, gradual release of MMF through perfusion of the allograft, at the time of harvest with MMF-NP. Our data indicates that perfusion of allograft heart with MMF-NP prior to transplantation suppresses the early intra-graft immune response and abrogates chronic allograft rejection.

Materials and Methods:

NP incubation with HUVEC cells

HUVEC cells were plated in 4-well Chambered Nunc™ Lab-Tek™ II chamber slides overnight. Then, CF660-NP suspensions were added to different wells and incubated for 1 hr in a humidified 37°C, 5% CO_2 incubator. The cells were washed with PBS three times and stained with DAPI and Lysotracker (Lysotracker® Green DND-26).

HUVEC cells viability assessment

HUVEC cells were cultured in 6-well plates overnight (0.5×10^6 cells/ml). Empty NPs or MMF-NPs were added to the HUVEC cells at concentrations similar to what was used *in vivo*. The samples were incubated in a humidified 37°C, 5% CO_2 incubator in triplicates for 24, 48 and 72 hours. Cells cultured without any additional reagent were considered as control. Cells were washed three times with PBS at the end of incubation time and dead cells were stained using eBioscience™ Fixable Viability Dye eFluor™ 450 (cat# 65–0863-14). The cell suspension was analyzed using a FACS Canto II (BD Bioscience, Franklin Lakes, NJ) instrument.

Preparation and characterization of MMF-NP

We have engineered MMF-NP using a single emulsion and solvent evaporation method. Briefly, Poly(D,L-lactic-co-glycolic) acid copolymer (PLGA) was dissolved in ethyl acetate and mixed with MMF® (in acetone). The mix was then emulsified in 3 mL of deionized water using probe sonication and homogenization over ice. The emulsion was added dropwise to 20 mL of deionized water and stirred for two hours to evaporate the organic solvent. After solvent evaporation, the MMF-NP was collected and washed by centrifugation using Amicon Ultra-15 centrifugal filter units (MWCO 100 kDa) at 3000 x g for 30 minutes. The size and zeta potential of MMF-NP were assessed and characterized using Dynamic Light Scattering (DLS). The morphology of MMF-NP was studied using scanning electron microscopy (SEM) and transmission electron microscopy (TEM). The filtrate of the MMF-NP wash steps were collected and the absorbances was then analyzed at 300 nm using a UV/VIS spectrophotometer. The amount of MMF in the filtrate was quantified by comparing the absorbance at 300 nm with a calibration curve of various concentrations of MMF.

The loading efficiency was calculated as following:

Loading Efficiency (%) = (MMFi-MMFf)/MMFi

Where MMFi is the initial amount of MMF used to prepare MMF-NP and MMFf is the free non-loaded MMF determined in the last step.

Release profile of MMF from MMF-NP

To quantify the release profile of MMF from NP, the MMF-NP solutions were incubated in triplicates at 37°C and assessed at defined time intervals (1, 2, and 4 hrs; 1, 2, 3, 4, 7 and 14 days). The samples were centrifuged at each time point using Amicon Ultra-15 centrifugal filter units (MWCO 10 kDa; Sigma-Aldrich) at 3,000 × g for 15 min. The absorbances of the filtrate and MMF-NP suspension were then analyzed at 300 nm using a UV/VIS spectrophotometer. The amount of released MMF at each time point was quantified by comparing the absorbance at 300 nm with a calibration curve of various concentrations of MMF.

T cell proliferation assay

Splenocytes were isolated from the spleens of C57BL/6 mice and seeded at one million cells per well in a round-bottom 96-well plate. Next, cells were stimulated using anti-mouse CD3/CD28 antibodies (3μg/ml in complete RPMI media). Free MMF and MMF-NP (freshly prepared, and 7 and 14 days post-MMF release experiment) were added to the cells. Unstimulated splenocytes were used as the negative control, and splenocytes stimulated with anti-mouse CD3/CD28 without the addition of MMF or MMF-NP were used as the positive control. The plate was placed in a humidified 37°C, 5% CO_2 incubator for 2 days. Next, tritiated thymidine (^3H) was added to each well, and the plate was returned to the incubator for 14 hrs. Cells were harvested using a semi-automated sample harvester and analyzed using a β scintillation counter.

Labeling of mycophenolic acid

Mycophenolic acid (MPA) (10 mM) was prepared in a 4 mL vial dried under high vacuum for 24 hours and dissolved in 100 μL of dimethylformamide (DMF) with (1H-benzotriazol-1-yl)-1,1,3,3-tetramethyluronium hexauorophosphate (HBTU) (12 mM, 1.2 eq). The solution was stirred at RT under argon for 30 min. Then, the amine-functionalized dye (Amine CF594) dissolved in 200 μL of anhydrous DMF with the concentration of 11 mM was added into reaction mixture. To activate coupling reaction, 2 μL of triethylamine (1.2 μmol, 1.2 eq) was added into solution and stirred for 4 hours. To quench the reaction, reaction mixture was directly dried under high vacuum for 2 hours. The mixture was diluted with 300 μL of methanol and 5 μL of solution was injected into LC/MS (Agilent 1200, USA) with a gradient reversed phase system (10% to 100% ACN/H_2O with 0.1% formic acid for 20 min) using Phenomenex Luna 5 μm C_{18} (2) column (100 × 4.6 mm, flow rate; 0.7 mL/min, monitoring of absorption; 245, 320, and 600 nm). The labeled MPA product (MPA*) was purified by reversed phase HPLC (Phenomenex Luna 5 μm C_{18} (2) column of 250 × 10.0 mm, flow rate; 2 mL/min, monitoring of absorption; 254, 320, and 600 nm) with a gradient solvent system (15% to 75% ACN/H_2O with 0.1% formic acid for 40 min).

Cell line and Mice

HUVEC cells (CRL-1730™) were purchased from ATCC®. C57BL/6J (JAX#000664) and B6(C)-H2-Ab1^{bm12}/KhEgJ (BM12, JAX#001162) were obtained from the Jackson Laboratory. Male or female mice were used at 7–8 weeks of age and were housed in sterilized and ventilated cages in a specific pathogen-free animal facility under a standard 12 hours light/12 hours dark cycle. Mice were fed irradiated food and water *ad libitum*. Each individual experiment was performed using three to four mice per group. All animal experiments and methods were performed in accordance with the relevant guidelines and regulations approved by the Institutional Animal Care and Use Committee of Brigham and Women's Hospital, Boston, MA.

Mouse heterotopic cardiac transplantation

Vascularized intra-abdominal heterotopic transplantation of heart allografts was performed using microsurgical techniques[22-23]. 1 mL of cold heparin (BD Vacutainer Sodium Heparin #366480, 143USP units/10 mL) was infused into the inferior vena cava (IVC) of the donor mouse. After heparin perfusion, either PBS (Control), free MMF, or MMF-NP was infused into the heart from the IVC. The heart was harvested following ligation/dissection of the superior vena cava (SVC) and IVC, and dissection of ascending aorta and pulmonary artery. Harvested donor heart was stored at 4°C and immersed in UW (University of Wisconsin) solution for two hours. After abdominal incision of recipient mouse, abdominal aorta and IVC were clamped. Ascending aorta and pulmonary artery of donor heart were sutured to abdominal aorta and IVC of recipient mouse, respectively, using 10–0 suture. Beating of transplanted heart was observed upon removal of cross clamp, and abdominal incision was closed by 6–0 suture. The survival of cardiac allografts was assessed by daily palpation.

Immunohistochemistry and immunofluorescence

Heart grafts harvested at designated time points post-transplantation were fixed in formalin and embedded in a paraffin block, or they were preserved in Optima Cutting Temperature (OCT) compound (Tissue-Tek, Torrance, CA) and stored at −80 degrees Celsius. Samples were cut into 5 μm sections and stained with H&E (paraffin block section), and DAPI, anti-F-actin, anti-CD31, anti-CD3, anti-CD11b, fibronectin, VCAM, ICAM and P-selectin for immunofluorescence (OCT block section).

Histological assessment of the allograft heart

Histological evaluation from H&E slides was done using a score modified from the International Society for Heart and Lung Transplantation[95-96]. Cellular infiltration was graded blindly from 0 to 4 from 6 random microscopic fields of each heart section (3 sections/heart, 4 mice per group). The grades were defined as follows: grade 0 (no cellular infiltration), grade 1 (less than 25% cellular infiltration), grade 2 (25% to 50% cellular infiltration), grade 3 (50% to 75% cellular infiltration) and grade 4 (more than 75% cellular infiltration with hemorrhage and/or fibrosis). Vascular appearance was determined by a combination of vascular occlusion score and perivascular cellular infiltration. Vascular (artery) occlusion was scored from grade 0 to 3 for every artery (3 sections/heart, 4 mice per group). The grades were defined as follows: grade 0 (no or minimal occlusion, <10%), grade 1 (10–25% occlusion), grade 2 (25% to 75% occlusion) and grade 3 (more than 75% occlusion). The perivascular cellular infiltration was scored as follows: grade 0 (no cellular infiltration around artery), grade 1 (less than 25% cellular infiltration around artery), grade 2 (25% to 75% cellular infiltration around artery) and grade 3 (more than 75% cellular infiltration around artery). Then, the sum of the vascular occlusion score and perivascular cellular infiltration score was designated as the vascular appearance score.

Flow cytometry

Flow cytometric analysis was performed of spleen and DLN, and each leukocyte population was quantified. All antibodies were purchased from BD (Becton Dickinson, Franklin Lakes, NJ). Cells were run on a FACS Canto II (BD Bioscience, Franklin Lakes, NJ) instrument. Data were analyzed by using FlowJo software.

DSA assay

The level of circulating donor specific antibody (DSA)-IgG in recipient mice serum were assessed by flow cytometry. Recipient serum were incubated with donor splenocytes at 37 degrees for 30 minutes, washed and incubated with FITC-conjugated goat antibody specific for the Fc portion of mouse IgG (Fc blocking antibody) at 4 degrees for 1 hour. After staining, the cells were washed, fixed in PBS containing 1% formalin and analyzed by flow cytometry as mean fluorescence intensity to reflect individual serum DSA-IgG levels.

HUVEC cells gene expression assessment

HUVEC cells were stimulated by TNFα (10ng/ml) and cultured in 6-well plates overnight (0.5×10^6 cells/ml). Either PBS, free MMF or MMF-NP were added to the HUVEC cells at concentrations similar to what was used *in vivo*. The samples were incubated in a humidified

37°C, 5% CO_2 incubator in triplicates for 24 hours. Cells were washed three times with PBS and the cell suspension was analyzed by qPCR.

Elispot assay

We followed the manufacturer's instructions (BD Biosciences). Immunospot plates (Millipore) were coated with IFNγ primary antibody for three hours in 37 degrees. Donor (BM12) splenocytes were irradiated at 3000 rads and plated with recipients' (C57BL/6) splenocytes in a 1:1 ratio and incubated in 37 degrees for 24 hours. Cells were washed out and the secondary antibody was added and incubated overnight. After development with the chromogen, the total number of spots per well were quantified using an ImmunoSpot Analyzer (Cellular Technology, Cleveland, OH, USA).

Mixed lymphocyte reaction (MLR) assay

Irradiated donor (BM12) splenocyte stimulators and recipient (C57BL/6) splenocyte responders were added to each well in a 96-well round bottom plate and incubated in 37 degrees for 2 days. 1μCi of tritiated thymidine (^3H) was added and the plate was incubated for additional 14 hours. The plate was run on cell Harvester96®, TOMTEC.

Quantitative PCR (qPCR)

RNA was isolated with TRIZOL (Invitrogen), and cDNA was synthesized using 2μg of RNA and High-Capacity Reverse Transcriptase (Invitrogen). RT-PCR was performed with SYBR Green PCR reagents on a Biorad detection system. RNA levels were normalized to the level of GAPDH and calculated as delta-delta threshold cycle (ΔΔCT). Primers used for RT-PCR are listed as below: GAPDH-F: GTTGTCTCCTGCGACTTCA, GAPDH-R: GGTGGTCCAGGGTTTCTTA; IL2-F: TGAGCAGGATGGAGAATTACAGG, IL2-R: GTCCAAGTTCATCTTCTAGGCAC, IL6-F: CTCTGGGAAATCGTGGAAAT, IL6-R: CCAGTTTGGTAGCATCCATC, TNFα-F: ATGAGAAGTTCCCAAATGGC, TNFα-R: CTCCACTTGGTGGTTTGCTA, IFNγ-F: TTGAGGTCAACAACCCACAG, IFNγ-R: TCAGCAGCGACTCCTTTTC, IL17-F: AAGGCAGCAGCGATCATCC, IL17-R: GGAACGGTTGAGGTAGTCTGAG, CCL2-F: GAAGGAATGGGTCCAGACAT, CCL2-R: ACGGGTCAACTTCACATTCA, CCR2-F: ACACCCTGTTTCGCTGTAGG, CCR2-R: GATTCCTGGAAGGTGGTCAA, CCL5-F: AGATCTCTGCAGCTGCCCTCA, CCL5-R: GGAGCACTTGCTGCTGGTGTAG, CCR5-F: GCTGCCTAAACCCTGTCATC, CCR5-R: GTTCTCCTGTGGATCGGGTA, CXCL9-F: CCGAGGCACGATCCACTAC, CXCL9-R: AGGCAGGTTTGATCTCCGTT, CXCL10-F: CAAGTGCTGCCGTCATTTTCT, CXCL10-R: ATAGGCTCGCAGGGATGATT, CXCR3-F: TACCTTGAGGTTAGTGAACGTCA, CXCR3-R: CGCTCTCGTTTTCCCCATAATC. VCAM-F: GTCAAAGAACTACAAGTCTA, VCAM-R: CTTCATTATCTAACTTCCTG, ICAM-F: GCAGTGACTCTGTGTCAG, ICAM-R: GGATCTGGTCCGCTAGCTC, P-selectin-F: TCGGTACCTTGACGTACC, P-selectin-R: CATGGATCCATTCTCAGG, hu-VCAM-F: CTACGCTGACAATGAATCCTG, hu-VCAM-R: GCAACTGAACACTTGACTGTG, hu-ICAM-F: CGTGTACTGGACTCCAGA, hu-ICAM-R: CACCGTGGTCGTGACCTC, hu-P-selectin-F: GCACTGACGGGTACCAAG, hu-P-selectin-R: TGCAGCTAGACTGATGCTG. All RT-PCR reactions were performed in triplicate.

Statistics

Data analysis was performed by using GraphPad Prism (GraphPad Software, Inc., San Diego, CA). Differences between groups were evaluated by ANOVA to determine significance. Significant difference was considered as *p<0.05, **p<0.01 and ***p<0.001.

Supplementary Material

Refer to Web version on PubMed Central for supplementary material.

Acknowledgements

This work is supported by the National Institute of Health (NIH) under Award Number RO1AI1296596 and RO1HL141815 (R.A.) and Brigham Research Institute Stepping Strong Innovator Award (R.A.) and BWH Health & Technology Innovation Fund (R.A.).

References:

1. Ojo AO; Hanson JA; Wolfe RA; Leichtman AB; Agodoa LY; Port FK, Long-term survival in renal transplant recipients with graft function. Kidney international 2000, 57 (1), 307–13. [PubMed: 10620213]
2. Prakash J; Ghosh B; Singh S; Soni A; Rathore SS, Causes of death in renal transplant recipients with functioning allograft. Indian J Nephrol 2012, 22 (4), 264–8. [PubMed: 23162269]
3. Bamoulid J; Staeck O; Halleck F; Khadzhynov D; Brakemeier S; Durr M; Budde K, The need for minimization strategies: current problems of immunosuppression. Transpl Int 2015, 28 (8), 891–900. [PubMed: 25752992]
4. Vincenti F; Friman S; Scheuermann E; Rostaing L; Jenssen T; Campistol JM; Uchida K; Pescovitz MD; Marchetti P; Tuncer M; Citterio F; Wiecek A; Chadban S; El-Shahawy M; Budde K; Goto N; Investigators D, Results of an international, randomized trial comparing glucose metabolism disorders and outcome with cyclosporine versus tacrolimus. Am J Transplant 2007, 7 (6), 1506–14. [PubMed: 17359512]
5. Silva HT Jr.; Yang HC; Meier-Kriesche HU; Croy R; Holman J; Fitzsimmons WE; First MR, Long-term follow-up of a phase III clinical trial comparing tacrolimus extended-release/MMF, tacrolimus/MMF, and cyclosporine/MMF in de novo kidney transplant recipients. Transplantation 2014, 97 (6), 636–41. [PubMed: 24521771]
6. Haller M; Oberbauer R, Calcineurin inhibitor minimization, withdrawal and avoidance protocols after kidney transplantation. Transpl Int 2009, 22 (1), 69–77. [PubMed: 18764837]
7. Srinivas TR; Meier-Kriesche HU, Minimizing immunosuppression, an alternative approach to reducing side effects: objectives and interim result. Clin J Am Soc Nephrol 2008, 3 Suppl 2, S101–16. [PubMed: 18308998]
8. Dean PG; Park WD; Cornell LD; Schinstock CA; Stegall MD, Early subclinical inflammation correlates with outcomes in positive crossmatch kidney allografts. Clin Transplant 2016, 30 (8), 925–33. [PubMed: 27225518]
9. van Besouw NM; Caliskan K; Peeters AM; Klepper M; Dieterich M; Maat LP; Weimar W; Manintveld OC; Baan CC, Interleukin-17-producing CD4(+) cells home to the graft early after human heart transplantation. J Heart Lung Transplant 2015, 34 (7), 933–40. [PubMed: 25682556]
10. Weiss S; Kotsch K; Francuski M; Reutzel-Selke A; Mantouvalou L; Klemz R; Kuecuek O; Jonas S; Wesslau C; Ulrich F; Pascher A; Volk HD; Tullius SG; Neuhaus P; Pratschke J, Brain death activates donor organs and is associated with a worse I/R injury after liver transplantation. Am J Transplant 2007, 7 (6), 1584–93. [PubMed: 17430397]
11. Uehara M; Solhjou Z; Banouni N; Kasinath V; Xiaqun Y; Dai L; Yilmam O; Yilmaz M; Ichimura T; Fiorina P; Martins PN; Ohori S; Guleria I; Maarouf OH; Tullius SG; McGrath MM; Abdi R, Ischemia augments alloimmune injury through IL-6-driven CD4(+) alloreactivity. Sci Rep 2018, 8 (1), 2461. [PubMed: 29410442]

12. Solhjou Z; Uehara M; Bahmani B; Maarouf OH; Ichimura T; Brooks CR; Xu W; Yilmaz M; Elkhal A; Tullius SG; Guleria I; McGrath MM; Abdi R, Novel Application of Localized Nanodelivery of Anti-Interleukin-6 Protects Organ Transplant From Ischemia-Reperfusion Injuries. Am J Transplant 2017, 17 (9), 2326–2337. [PubMed: 28296000]

13. Jurewicz M; Ueno T; Azzi J; Tanaka K; Murayama T; Yang S; Sayegh MH; Niimi M; Abdi R, Donor antioxidant strategy prolongs cardiac allograft survival by attenuating tissue dendritic cell immunogenicity(dagger). Am J Transplant 2011, 11 (2), 348–55. [PubMed: 21182586]

14. Kamaly N; Xiao Z; Valencia PM; Radovic-Moreno AF; Farokhzad OC, Targeted polymeric therapeutic nanoparticles: design, development and clinical translation. Chem Soc Rev 2012, 41 (7), 2971–3010. [PubMed: 22388185]

15. Shi J; Xiao Z; Kamaly N; Farokhzad OC, Self-assembled targeted nanoparticles: evolution of technologies and bench to bedside translation. Acc Chem Res 2011, 44 (10), 1123–34. [PubMed: 21692448]

16. Farokhzad OC, Nanotechnology for drug delivery: the perfect partnership. Expert opinion on drug delivery 2008, 5 (9), 927–9. [PubMed: 18754745]

17. Farokhzad OC; Langer R, Impact of nanotechnology on drug delivery. ACS nano 2009, 3 (1), 16–20. [PubMed: 19206243]

18. Ferrari M, Cancer nanotechnology: Opportunities and challenges. Nature Reviews Cancer 2005, 5 (3), 161–171. [PubMed: 15738981]

19. Heemann U; Kliem V; Budde K; Hamza A; Jurgensen JS; Juarez F; Arns W; Rath T; Haller H, Mycophenolate mofetil maintenance therapy in renal transplant patients: long-term results of the TranCept STAY study. Clin Transplant 2012, 26 (6), 919–26. [PubMed: 22994923]

20. Cui J; Qin L; Zhang J; Abrahimi P; Li H; Li G; Tietjen GT; Tellides G; Pober JS; Mark Saltzman W, Ex vivo pretreatment of human vessels with siRNA nanoparticles provides protein silencing in endothelial cells. Nat Commun 2017, 8 (1), 191. [PubMed: 28775323]

21. Tietjen GT; Hosgood SA; DiRito J; Cui J; Deep D; Song E; Kraehling JR; Piotrowski-Daspit AS; Kirkiles-Smith NC; Al-Lamki R; Thiru S; Bradley JA; Saeb-Parsy K; Bradley JR; Nicholson ML; Saltzman WM; Pober JS, Nanoparticle targeting to the endothelium during normothermic machine perfusion of human kidneys. Sci Transl Med 2017, 9 (418).

22. Bahmani B; Uehara M; Jiang L; Ordikhani F; Banouni N; Ichimura T; Solhjou Z; Furtmuller GJ; Brandacher G; Alvarez D; von Andrian UH; Uchimura K; Xu Q; Vohra I; Yilmam OA; Haik Y; Azzi J; Kasinath V; Bromberg JS; McGrath MM; Abdi R, Targeted delivery of immune therapeutics to lymph nodes prolongs cardiac allograft survival. J Clin Invest 2018, 128 (11), 4770–4786. [PubMed: 30277476]

23. Corry RJ; Winn HJ; Russell PS, Heart transplantation in congenic strains of mice. Transplant Proc 1973, 5 (1), 733–5. [PubMed: 4572133]

24. Khosroshahi HT; Shoja MM; Peyrovifar A; Hashemi SR; Amjadi M, Mycophenolate mofetil dose reduction in renal transplant recipients: a 5-year follow-up study. Transplant Proc 2009, 41 (7), 2797–9. [PubMed: 19765438]

25. Jorge S; Guerra J; Santana A; Mil-Homens C; Prata MM, Mycophenolate mofetil: ten years' experience of a renal transplant unit. Transplant Proc 2008, 40 (3), 700–4. [PubMed: 18454991]

26. Manito N; Rabago G; Palomo J; Arizon JM; Delgado J; Almenar L; Crespo-Leiro MG; Lage E; Pulpon L, Improvement in chronic renal failure after mycophenolate mofetil introduction and cyclosporine dose reduction: four-year results from a cohort of heart transplant recipients. Transplant Proc 2011, 43 (7), 2699–706. [PubMed: 21911149]

27. Allison AC; Eugui EM, Mechanisms of action of mycophenolate mofetil in preventing acute and chronic allograft rejection. Transplantation 2005, 80 (2 Suppl), S181–90. [PubMed: 16251851]

28. Klupp J; Dambrin C; Hibi K; Luna J; Suzuki T; Hausen B; Birsan T; Van Gelder T; Fitzgerald PJ; Berry G; Morris RE, Treatment by mycophenolate mofetil of advanced graft vascular disease in non-human primate recipients of orthotopic aortic allografts. Am J Transplant 2003, 3 (7), 817–29. [PubMed: 12814473]

29. Racusen LC; Regele H, The pathology of chronic allograft dysfunction. Kidney Int Suppl 2010, (119), S27–32. [PubMed: 21116314]

30. Chapman JR; O'Connell PJ; Nankivell BJ, Chronic renal allograft dysfunction. Journal of the American Society of Nephrology : JASN 2005, 16 (10), 3015–26. [PubMed: 16120819]

31. Merola J; Jane-Wit DD; Pober JS, Recent advances in allograft vasculopathy. Curr Opin Organ Transplant 2017, 22 (1), 1–7. [PubMed: 27898462]

32. Okada M; Wang CY; Hwang DW; Sakaguchi T; Olson KE; Yoshikawa Y; Minamoto K; Mazer SP; Yan SF; Pinsky DJ, Transcriptional control of cardiac allograft vasculopathy by early growth response gene-1 (Egr-1). Circ Res 2002, 91 (2), 135–42. [PubMed: 12142346]

33. Durrbach A; Pestana JM; Pearson T; Vincenti F; Garcia VD; Campistol J; Rial Mdel C; Florman S; Block A; Di Russo G; Xing J; Garg P; Grinyo J, A phase III study of belatacept versus cyclosporine in kidney transplants from extended criteria donors (BENEFIT-EXT study). Am J Transplant 2010, 10 (3), 547–57. [PubMed: 20415898]

34. Naesens M; Kuypers DR; Sarwal M, Calcineurin inhibitor nephrotoxicity. Clin J Am Soc Nephrol 2009, 4 (2), 481–508. [PubMed: 19218475]

35. Vincenti F, Immunosuppression minimization: current and future trends in transplant immunosuppression. Journal of the American Society of Nephrology : JASN 2003, 14 (7), 1940–8. [PubMed: 12819255]

36. Vincenti F; Larsen C; Durrbach A; Wekerle T; Nashan B; Blancho G; Lang P; Grinyo J; Halloran PF; Solez K; Hagerty D; Levy E; Zhou W; Natarajan K; Charpentier B; Belatacept Study G, Costimulation blockade with belatacept in renal transplantation. The New England journal of medicine 2005, 353 (8), 770–81. [PubMed: 16120857]

37. Meier-Kriesche HU; Baliga R; Kaplan B, Decreased renal function is a strong risk factor for cardiovascular death after renal transplantation. Transplantation 2003, 75 (8), 1291–5. [PubMed: 12717218]

38. Halloran PF, Immunosuppressive drugs for kidney transplantation. The New England journal of medicine 2004, 351 (26), 2715–29. [PubMed: 15616206]

39. Naesens M; Lerut E; Sarwal M; Van Damme B; Vanrenterghem Y; Kuypers DR, Balancing efficacy and toxicity of kidney transplant immunosuppression. Transplant Proc 2009, 41 (8), 3393–5. [PubMed: 19857756]

40. Gelman AE; Li W; Richardson SB; Zinselmeyer BH; Lai J; Okazaki M; Kornfeld CG; Kreisel FH; Sugimoto S; Tietjens JR; Dempster J; Patterson GA; Krupnick AS; Miller MJ; Kreisel D, Cutting edge: Acute lung allograft rejection is independent of secondary lymphoid organs. J Immunol 2009, 182 (7), 3969–73. [PubMed: 19299693]

41. Asaoka T; Marubashi S; Kobayashi S; Hama N; Eguchi H; Takeda Y; Tanemura M; Wada H; Takemasa I; Takahashi H; Ruiz P; Doki Y; Mori M; Nagano H, Intragraft transcriptome level of CXCL9 as biomarker of acute cellular rejection after liver transplantation. J Surg Res 2012, 178 (2), 1003–14. [PubMed: 22889476]

42. Enk AH; Angeloni VL; Udey MC; Katz SI, An essential role for Langerhans cell-derived IL-1 beta in the initiation of primary immune responses in skin. J Immunol 1993, 150 (9), 3698–704. [PubMed: 8473727]

43. Steinman RM; Inaba K; Turley S; Pierre P; Mellman I, Antigen capture, processing, and presentation by dendritic cells: recent cell biological studies. Hum Immunol 1999, 60 (7), 562–7. [PubMed: 10426272]

44. Kimber I; Cumberbatch M, Stimulation of Langerhans cell migration by tumor necrosis factor alpha (TNF-alpha). J Invest Dermatol 1992, 99 (5), 48S–50S. [PubMed: 1431209]

45. Jurewicz M; Takakura A; Augello A; Naini SM; Ichimura T; Zandi-Nejad K; Abdi R, Ischemic injury enhances dendritic cell immunogenicity via TLR4 and NF-kappa B activation. J Immunol 2010, 184 (6), 2939–48. [PubMed: 20164431]

46. Batal I; Azzi J; Mounayar M; Abdoli R; Moore R; Lee JY; Rosetti F; Wang C; Fiorina P; Sackstein R; Ichimura T; Abdi R, The mechanisms of up-regulation of dendritic cell activity by oxidative stress. Journal of leukocyte biology 2014, 96 (2), 283–93. [PubMed: 24676276]

47. Ingulli E, Mechanism of cellular rejection in transplantation. Pediatr Nephrol 2010, 25 (1), 61–74. [PubMed: 21476231]

48. Golshayan D; Lechler R, Commentary: Priming of alloreactive T cells--where does it happen? Eur J Immunol 2004, 34 (12), 3301–4. [PubMed: 15484195]

49. El-Sawy T; Miura M; Fairchild R, Early T cell response to allografts occurring prior to alloantigen priming up-regulates innate-mediated inflammation and graft necrosis. Am J Pathol 2004, 165 (1), 147–57. [PubMed: 15215170]
50. Su CA; Iida S; Abe T; Fairchild RL, Endogenous memory CD8 T cells directly mediate cardiac allograft rejection. Am J Transplant 2014, 14 (3), 568–79. [PubMed: 24502272]
51. Valujskikh A; Heeger PS, Emerging roles of endothelial cells in transplant rejection. Curr Opin Immunol 2003, 15 (5), 493–8. [PubMed: 14499255]
52. Biedermann BC; Pober JS, Human endothelial cells induce and regulate cytolytic T cell differentiation. J Immunol 1998, 161 (9), 4679–87. [PubMed: 9794397]
53. Briscoe DM; Alexander SI; Lichtman AH, Interactions between T lymphocytes and endothelial cells in allograft rejection. Curr Opin Immunol 1998, 10 (5), 525–31. [PubMed: 9794840]
54. Briscoe DM; Henault LE; Geehan C; Alexander SI; Lichtman AH, Human endothelial cell costimulation of T cell IFN-g production. J Immunol 1997, 159, 3247–3256. [PubMed: 9317123]
55. Marelli-Berg FM; Scott D; Bartok I; Peek E; Dyson J; Lechler RI, Activated murine endothelial cells have reduced immunogenicity for CD8+ T cells: a mechanism of immunoregulation? J Immunol 2000, 165 (8), 4182–9. [PubMed: 11035050]
56. Marelli-Berg FM; Scott D; Bartok I; Peek E; Dyson J; Lechler RI, Antigen presentation by murine endothelial cells. Transplant Proc 2001, 33 (1–2), 315–6. [PubMed: 11266836]
57. Herrera OB; Golshayan D; Tibbott R; Salcido Ochoa F; James MJ; Marelli-Berg FM; Lechler RI, A novel pathway of alloantigen presentation by dendritic cells. J Immunol 2004, 173 (8), 4828–37. [PubMed: 15470023]
58. Manes TD; Pober JS, Antigen presentation by human microvascular endothelial cells triggers ICAM-1-dependent transendothelial protrusion by, and fractalkine-dependent transendothelial migration of, effector memory CD4+ T cells. J Immunol 2008, 180 (12), 8386–92. [PubMed: 18523306]
59. Pober JS; Kluger MS; Schechner JS, Human endothelial cell presentation of antigen and the homing of memory/effector T cells to skin. Ann N Y Acad Sci 2001, 941, 12–25. [PubMed: 11594565]
60. Pober JS; Merola J; Liu R; Manes TD, Antigen Presentation by Vascular Cells. Front Immunol 2017, 8, 1907. [PubMed: 29312357]
61. Denton MD; Geehan CS; Alexander SI; Sayegh MH; Briscoe DM, Endothelial cells modify the costimulatory capacity of transmigrating leukocytes and promote CD28-mediated CD4+ T cell alloactivation. J Exp Med 1999, 190 (4), 555–66. [PubMed: 10449526]
62. Denton MD; Geehan CS; Alexander SI; Sayegh MH; Briscoe DM, Endothelial cells modify the costimulatory capacity of transmigrating leukocytes and promote CD28-mediated CD4(+) T cell alloactivation. J Exp Med 1999, 190 (4), 555–66. [PubMed: 10449526]
63. Tietjen GT; Bracaglia LG; Saltzman WM; Pober JS, Focus on Fundamentals: Achieving Effective Nanoparticle Targeting. Trends Mol Med 2018, 24 (7), 598–606. [PubMed: 29884540]
64. Allison AC; Hovi T; Watts RW; Webster AD, The role of de novo purine synthesis in lymphocyte transformation. Ciba Found Symp 1977, (48), 207–24. [PubMed: 415850]
65. Srinivas TR; Kaplan B; Schold JD; Meier-Kriesche HU, The impact of mycophenolate mofetil on long-term outcomes in kidney transplantation. Transplantation 2005, 80 (2 Suppl), S211–20. [PubMed: 16251854]
66. Kitchin JE; Pomeranz MK; Pak G; Washenik K; Shupack JL, Rediscovering mycophenolic acid: a review of its mechanism, side effects, and potential uses. J Am Acad Dermatol 1997, 37 (3 Pt 1), 445–9. [PubMed: 9308561]
67. Blaheta RA; Leckel K; Wittig B; Zenker D; Oppermann E; Harder S; Scholz M; Weber S; Schuldes H; Encke A; Markus BH, Inhibition of endothelial receptor expression and of T-cell ligand activity by mycophenolate mofetil. Transpl Immunol 1998, 6 (4), 251–9. [PubMed: 10342739]
68. Glomsda BA; Blaheta RA; Hailer NP, Inhibition of monocyte/endothelial cell interactions and monocyte adhesion molecule expression by the immunosuppressant mycophenolate mofetil. Spinal Cord 2003, 41 (11), 610–9. [PubMed: 14569262]

69. Hoffmann J; Bohm M; Abele-Ohl S; Ramsperger-Gleixner M; Spriewald BM; Zinser E; Steinkasserer A; Weyand M; Ensminger SM, Reduction of transplant arteriosclerosis after treatment with mycophenolate mofetil and ganciclovir in a mouse aortic allograft model. Exp Clin Transplant 2012, 10 (6), 592–600. [PubMed: 23110396]
70. Shimizu H; Takahashi M; Takeda S; Inoue S; Fujishiro J; Hakamata Y; Kaneko T; Murakami T; Takeuchi K; Takeyoshi I; Morishita Y; Kobayashi E, Mycophenolate mofetil prevents transplant arteriosclerosis by direct inhibition of vascular smooth muscle cell proliferation. Transplantation 2004, 77 (11), 1661–7. [PubMed: 15201664]
71. Devalliere J; Chang WG; Andrejecsk JW; Abrahimi P; Cheng CJ; Jane-wit D; Saltzman WM; Pober JS, Sustained delivery of proangiogenic microRNA-132 by nanoparticle transfection improves endothelial cell transplantation. FASEB J 2014, 28 (2), 908–22. [PubMed: 24221087]
72. Liang Y; Christopher K; Finn PW; Colson YL; Perkins DL, Graft produced interleukin-6 functions as a danger signal and promotes rejection after transplantation. Transplantation 2007, 84 (6), 771–7. [PubMed: 17893611]
73. Booth AJ; Grabauskiene S; Wood SC; Lu G; Burrell BE; Bishop DK, IL-6 promotes cardiac graft rejection mediated by CD4+ cells. J Immunol 2011, 187 (11), 5764–71. [PubMed: 22025555]
74. Diaz JA; Booth AJ; Lu G; Wood SC; Pinsky DJ; Bishop DK, Critical role for IL-6 in hypertrophy and fibrosis in chronic cardiac allograft rejection. Am J Transplant 2009, 9 (8), 1773–83. [PubMed: 19538487]
75. Zhao X; Boenisch O; Yeung M; Mfarrej B; Yang S; Turka LA; Sayegh MH; Iacomini J; Yuan X, Critical role of proinflammatory cytokine IL-6 in allograft rejection and tolerance. Am J Transplant 2012, 12 (1), 90–101. [PubMed: 21992708]
76. Kimura N; Itoh S; Nakae S; Axtell RC; Velotta JB; Bos EJ; Merk DR; Gong Y; Okamura H; Nagamine CM; Adachi H; Kornfeld H; Robbins RC; Fischbein MP, Interleukin-16 deficiency suppresses the development of chronic rejection in murine cardiac transplantation model. J Heart Lung Transplant 2011, 30 (12), 1409–17. [PubMed: 22055099]
77. Fogal B; Yi T; Wang C; Rao DA; Lebastchi A; Kulkarni S; Tellides G; Pober JS, Neutralizing IL-6 reduces human arterial allograft rejection by allowing emergence of CD161+ CD4+ regulatory T cells. J Immunol 2011, 187 (12), 6268–80. [PubMed: 22084439]
78. Collins T; Read MA; Neish AS; Whitley MZ; Thanos D; Maniatis T, Transcriptional regulation of endothelial cell adhesion molecules: NF-kappa B and cytokine-inducible enhancers. FASEB J 1995, 9 (10), 899–909. [PubMed: 7542214]
79. Chen Q; Fisher DT; Clancy KA; Gauguet JM; Wang WC; Unger E; Rose-John S; von Andrian UH; Baumann H; Evans SS, Fever-range thermal stress promotes lymphocyte trafficking across high endothelial venules via an interleukin 6 trans-signaling mechanism. Nat Immunol 2006, 7 (12), 1299–308. [PubMed: 17086187]
80. Roebuck KA; Finnegan A, Regulation of intercellular adhesion molecule-1 (CD54) gene expression. Journal of leukocyte biology 1999, 66 (6), 876–88. [PubMed: 10614768]
81. Baggiolini M, Chemokines and leukocyte traffic. Nature 1998, 392 (6676), 565–8. [PubMed: 9560152]
82. Jane-Wit D; Manes TD; Yi T; Qin L; Clark P; Kirkiles-Smith NC; Abrahimi P; Devalliere J; Moeckel G; Kulkarni S; Tellides G; Pober JS, Alloantibody and complement promote T cell-mediated cardiac allograft vasculopathy through noncanonical nuclear factor-kappaB signaling in endothelial cells. Circulation 2013, 128 (23), 2504–16. [PubMed: 24045046]
83. Chong AS; Alegre ML; Miller ML; Fairchild RL, Lessons and limits of mouse models. Cold Spring Harb Perspect Med 2013, 3 (12), a015495. [PubMed: 24296351]
84. von Horn C; Minor T, Isolated kidney perfusion: the influence of pulsatile flow. Scand J Clin Lab Invest 2018, 1–5. [PubMed: 29148292]
85. Werner NL; Alghanem F; Rakestraw SL; Sarver DC; Nicely B; Pietroski RE; Lange P; Rudich SM; Mendias CL; Rojas-Pena A; Magee JC; Bartlett RH; Ozer K, Ex Situ Perfusion of Human Limb Allografts for 24 Hours. Transplantation 2017, 101 (3), e68–e74. [PubMed: 28222055]
86. Hosgood SA; Shah K; Patel M; Nicholson ML, The effect of prolonged of warm ischaemic injury on renal function in an experimental ex vivo normothermic perfusion system. J Transl Med 2015, 13, 207. [PubMed: 26123198]

87. Patel K; Atkinson C; Tran D; Nadig SN, Nanotechnological Approaches to Immunosuppression and Tolerance Induction. Curr Transplant Rep 2017, 4 (2), 159–168. [PubMed: 29057203]

88. Zhu P; Atkinson C; Dixit S; Cheng Q; Tran D; Patel K; Jiang YL; Esckilsen S; Miller K; Bazzle G; Allen P; Moore A; Broome AM; Nadig SN, Organ preservation with targeted rapamycin nanoparticles: a pre-treatment strategy preventing chronic rejection in vivo. RSC Adv 2018, 8 (46), 25909–25919. [PubMed: 30220998]

89. Nadig SN; Dixit SK; Levey N; Esckilsen S; Miller K; Dennis W; Atkinson C; Broome AM, Immunosuppressive nano-therapeutic micelles downregulate endothelial cell inflammation and immunogenicity. RSC Adv 2015, 5 (54), 43552–43562. [PubMed: 26167278]

90. Dong Y; Feng SS, Poly(d,l-lactide-co-glycolide)/montmorillonite nanoparticles for oral delivery of anticancer drugs. Biomaterials 2005, 26 (30), 6068–76. [PubMed: 15894372]

91. Kim DH; Martin DC, Sustained release of dexamethasone from hydrophilic matrices using PLGA nanoparticles for neural drug delivery. Biomaterials 2006, 27 (15), 3031–7. [PubMed: 16443270]

92. Aguado MT; Lambert PH, Controlled-release vaccines--biodegradable polylactide/polyglycolide (PL/PG) microspheres as antigen vehicles. Immunobiology 1992, 184 (2–3), 113–25. [PubMed: 1587538]

93. Kelly RJ, Clinical and laboratory evaluation of a new synthetic absorbable suture. Rev Surg 1970, 27 (2), 142–3. [PubMed: 5446536]

94. Blanco E; Shen H; Ferrari M, Principles of nanoparticle design for overcoming biological barriers to drug delivery. Nat Biotechnol 2015, 33 (9), 941–51. [PubMed: 26348965]

95. Billingham ME; Cary NR; Hammond ME; Kemnitz J; Marboe C; McCallister HA; Snovar DC; Winters GL; Zerbe A, A working formulation for the standardization of nomenclature in the diagnosis of heart and lung rejection: Heart Rejection Study Group. The International Society for Heart Transplantation. J Heart Transplant 1990, 9 (6), 587–93. [PubMed: 2277293]

96. Stewart S; Winters GL; Fishbein MC; Tazelaar HD; Kobashigawa J; Abrams J; Andersen CB; Angelini A; Berry GJ; Burke MM; Demetris AJ; Hammond E; Itescu S; Marboe CC; McManus B; Reed EF; Reinsmoen NL; Rodriguez ER; Rose AG; Rose M; Suciu-Focia N; Zeevi A; Billingham ME, Revision of the 1990 working formulation for the standardization of nomenclature in the diagnosis of heart rejection. J Heart Lung Transplant 2005, 24 (11), 1710–20. [PubMed: 16297770]

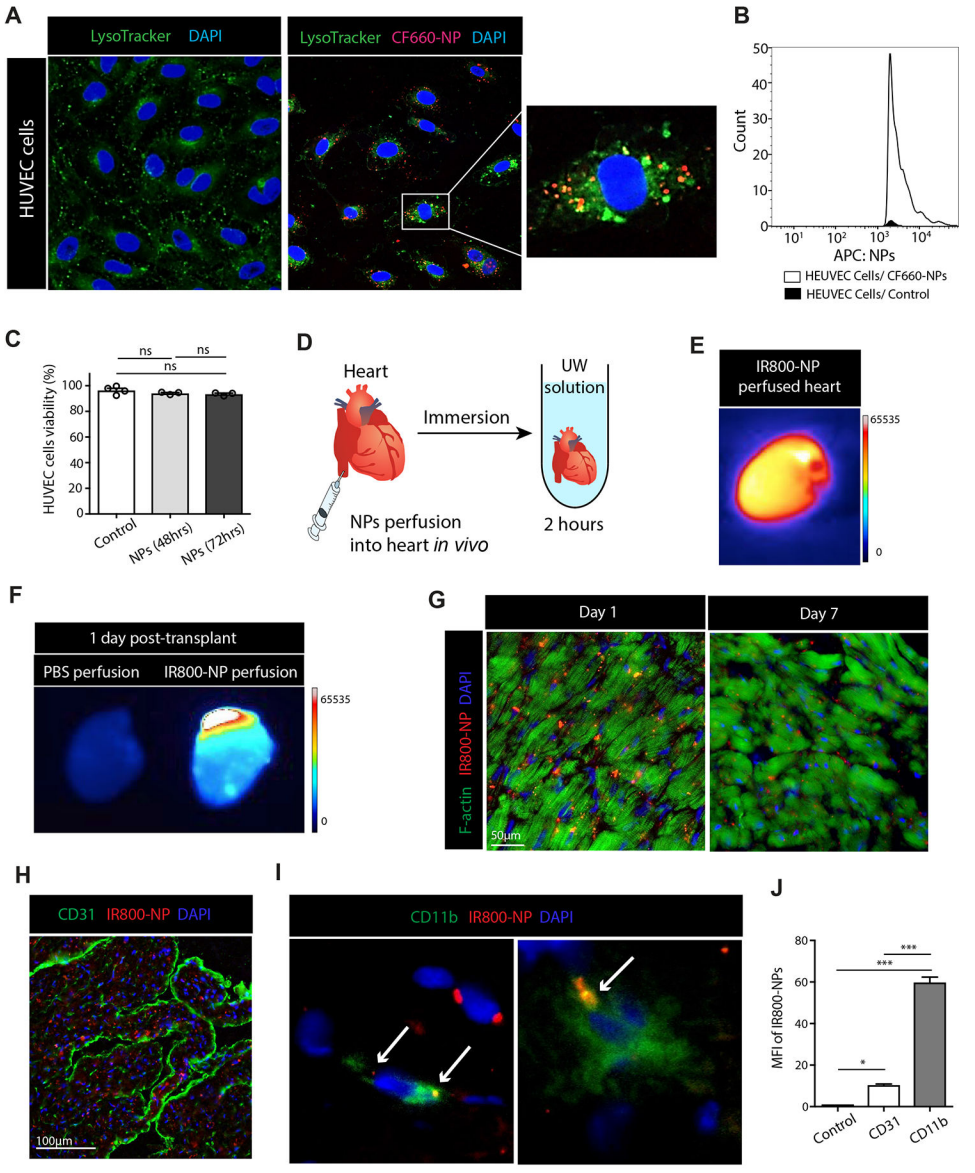

Figure 1. Cellular uptake and organ delivery of PEG-PLGA nanoparticle *in vivo* and *in vitro*.

(A) HUVEC cells were used to assess uptake of CF660-labeled PEG-PLGA nanoparticle (CF660-NP, red). Lysosomes were stained by LysoTracker® (green) dye, and cell nuclei were stained using DAPI (blue). Fluorescence confocal imaging of the HUVEC cells 1 hour post-incubation with CF660-NP showed significant uptake. CF660-NPs were detected inside HUVEC cells. (B) Histogram of FACS analysis showed a high count of CF660-NPs in HUVEC cells. (C) No differences were seen in HUVEC cell viability at 48 and 72 hours incubation compared to control, as assessed by flow cytometry. (D) The mouse heart was perfused with IR800-labeled PEG-PLGA nanoparticle (IR800-NP) from inferior vena cava (IVC) and immersed in UW (University of Wisconsin) solution for 2 hours at 4 degrees Celsius. (E) Hearts perfused with IR800-NP were imaged by UVP iBox® Explorer imaging microscope and a strong fluorescent signal was detected. (F) Hearts perfused with either PBS or IR800-NP were transplanted into recipient mice and harvested on the next day. The

heart perfused with IR800-NP showed a strong fluorescent signal in contrast to the PBS-perfused heart. (G) The heart perfused with IR800-NP (red) was assessed histologically 1 day and 7 days post-transplant. Many IR800-NPs were detected between myocytes (F-actin, green) at day 1 and IR800-NPs were still detectable 7 days post-transplant. DAPI was used to stain cell nuclei (blue). (H) IR800-NPs were observed outside the vasculature (CD31, green) at day 1 post-transplant. (I) IR800-NP were found inside the cytoplasm of $CD11b^{+}$ cells and some $CD11b^{-}$ cells at 1 day post-transplant. (J) At day 1 post-transplant, intra-allograft mean fluorescent intensity (MFI) of IR800-NPs was significantly higher in $CD11b^{+}$ cells compared to CD31 (Control vs. CD31 vs. CD11b, 1.1±0.01 vs. 10.4±0.5 vs. 59.8±2.6, ***$p<0.001$, n=3/group).

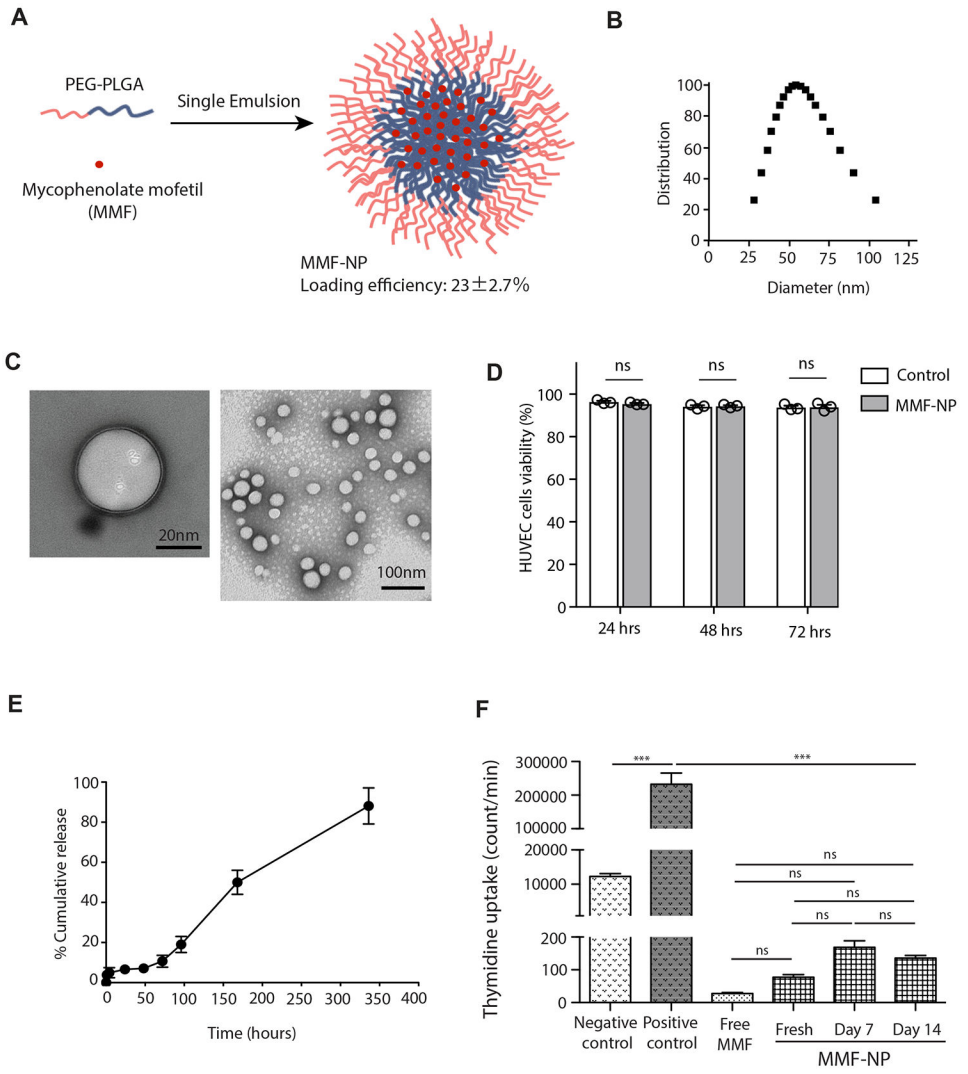

Figure 2. Synthesis and characterization of MMF-NP.

(A) Schematic of MMF-NP fabrication. (B) Dynamic light scattering measurements (DLS) of MMF-NP. (C) TEM image of NPs (stained with 3% uranyl acetate). (D) HUVEC cells viability incubated with MMF-NP showed no difference in 24, 48 and 72 hours compared to control. (E) *In vitro* release profile of MMF from NP. (F) T cell stimulation assay either with control, free MMF or MMF-NP (freshly prepared, 7 days and 14 days post-MMF release experiment). MMF-NP suppressed T cell proliferation, as measured by thymidine incorporation, with no differences between fresh, 7 days and 14 days post-MMF release. Unstimulated splenocytes were used as the negative control, and splenocytes stimulated with anti-mouse CD3/CD28 were used as the positive control.

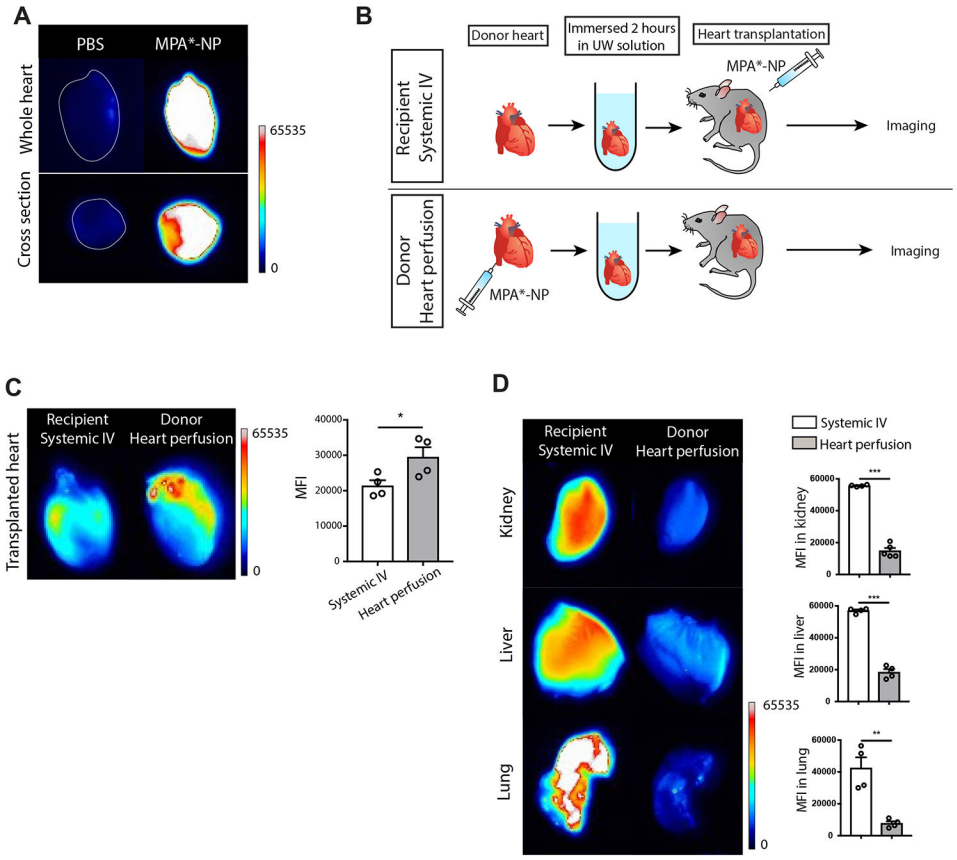

Figure 3. Biodistribution of MPA*-NP.

(A) The heart perfused with MPA*-NP showed high signal in whole image and cross section image compared to the heart perfused with PBS. (B) The schema describing two group study designs. MPA*-NP was injected intravenously into recipient mice in recipient systemic IV group. MPA*-NP was perfused into donor heart and the perfused heart was transplanted into recipient mice. (C) The allograft heart in donor heart perfusion group showed significantly higher MPA*-NP signal compared to allograft heart in recipient systemic IV group (recipient systemic IV vs. donor heart perfusion, 21401±1560 vs. 29526±2742, *p<0.05, n=4mice/group). (D) Kidney, liver and lung harvested from donor heart perfusion group showed significantly lower MPA*-NP signal compared to recipient systemic IV group (recipient systemic IV vs. donor heart perfusion, 55689±289 vs. 14806±1810, ***p<0.001 for kidney, 56995±788 vs. 18375±1995, ***p<0.001 for liver, 42411±5743 vs. 7712±1330, **p<0.01 for lung, n=4mice/group).

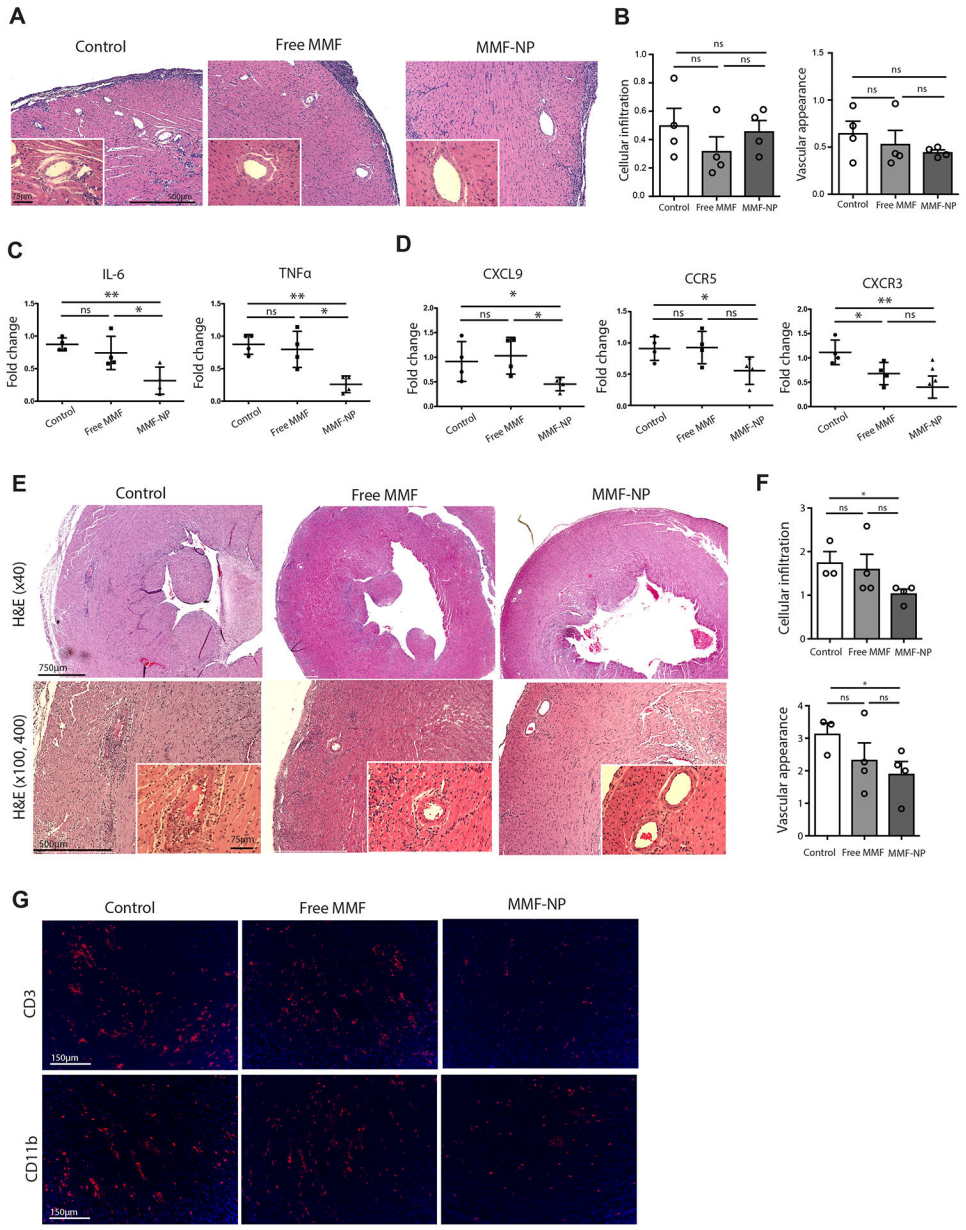

Figure 4. Early intra-graft immune response suppression by MMF-NP.

(A) H&E staining of the allograft hearts perfused with PBS (control), free MMF or MMF-NP 5 days post-transplantation. No difference in light microscopic evidence of rejection, including cellular infiltration or vascular injury was detected in heart grafts among the three groups. (B) No difference of cellular infiltration and vascular appearance score was found among the three groups (control vs. free MMF vs. MMF-NP, 0.50±0.12 vs. 0.32±0.61 vs. 0.45±0.07 for cellular infiltration, 0.65±0.13 vs. 0.53±0.14 vs. 0.45±0.02 for vascular appearance score, n=4mice/group). (C) The analysis of heart allografts by qPCR showed significantly lower expression of IL-6 and TNFα in the heart grafts perfused with MMF-NP compared to the control and free MMF groups (control vs. free MMF vs. MMF-NP, 0.87±0.05 vs. 0.74±0.13 vs. 0.31±0.10 for IL-6, 0.87±0.07 vs. 0.79±0.14 vs. 0.25±0.06 for

TNFα, n=4mice/group). (D) The expression of CXCL9 was reduced significantly in the heart allograft perfused with MMF-NP, as compared to the control and free MMF groups (control vs. free MMF vs. MMF-NP, 0.91±0.20 vs. 1.03±0.18 vs. 0.45±0.06 for CXCL9, n=4mice/group). A trend towards reduction was also observed for the expression of CCR5 and CXCR3 in the MMF-NP group (control vs. free MMF vs. MMF-NP, 0.91±0.09 vs. 0.92±0.12 vs. 0.55±0.10 for CCR5, 1.11±0.12 vs. 0.68±0.11 vs. 0.40±0.11 for CXCR3, n=4mice/group). (E) H&E staining of the heart allografts at 14 days post-transplant. Control heart showed moderate cellular infiltration of the myocytes and vasculopathy. Mild cellular infiltration of the myocytes and clear vasculature were observed in free MMF group. The heart graft perfused with MMF-NP had scant cellular infiltration of myocytes and clear vasculature. (F) The heart allograft perfused with MMF-NP showed significantly lower cellular infiltration and vascular appearance compared to control group. (control vs. free MMF vs. MMF-NP, 1.67±0.33 vs. 1.41±0.34 vs. 0.48±0.13 for cellular infiltration, 2.52±0.74 vs. 1.31±0.19 vs. 0.72±0.13 for vascular appearance score, n=3-4mice/group). (G) Very few $CD3^+$ T cells and $CD11b^+$ cells infiltrates were observed in the heart allograft perfused with MMF-NP, as compared to control and free MMF groups.

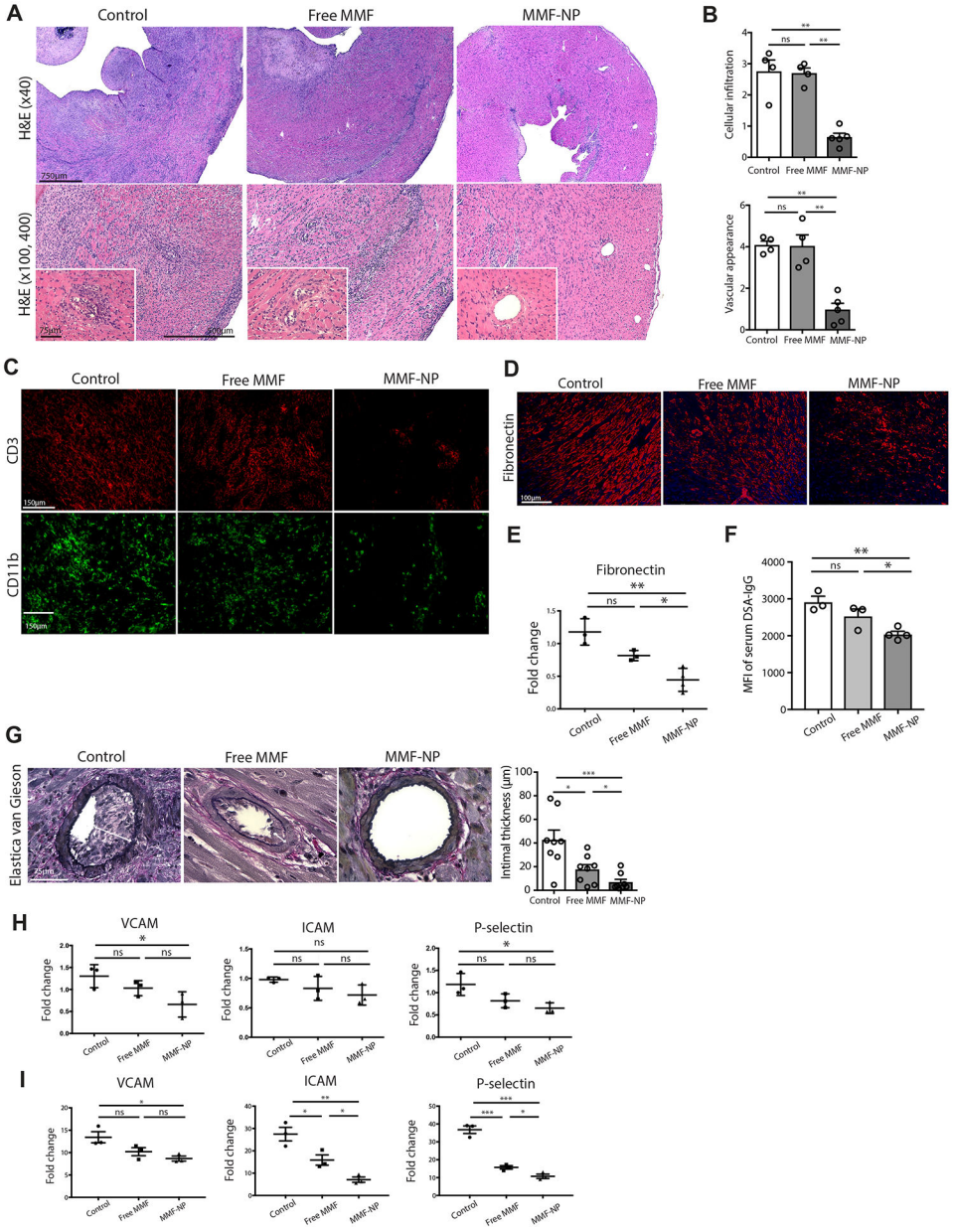

Figure 5. Perfusion of donor heart with MMF-NP prior to transplant showed marked effect within the graft and abrogated chronic rejection.

(A) H&E staining of the heart allografts at 28 days post-transplant. Control heart showed moderate to severe cellular infiltration and occluded vasculature. The heart graft perfused with free MMF showed moderate cellular infiltration and vasculopathy. The heart graft perfused with MMF-NP showed much lower cellular infiltration and intact vasculature. (B) The histological scoring of both cellular infiltration and vascular appearance showed significantly lower scores in the MMF-NP group, as compared to the control and free MMF group (control vs. free MMF vs. MMF-NP, 2.67±0.30 vs. 2.69±0.17 vs. 0.91±0.28 for cellular infiltration, 4.01±0.19 vs. 4.03±0.54 vs. 1.43±0.52 for vascular appearance score, n=4mice/group). (C) Very low infiltration of $CD3^+$ and $CD11b^+$ cells were observed in the

heart allograft perfused with MMF-NP in comparison to control and free MMF groups. (D) Fibronectin staining showed less fibrosis in MMF-NP group compared to control and free MMF groups. (E) Gene expression of fibronectin showed significantly less expression in the allograft heart harvested from MMF-NP group compared to control and free MMF groups (control vs. free MMF vs. MMF-NP, 1.2±0.12 vs. 0.8±0.04 vs. 0.4±0.08, n=3mice/group). (F) MFI of DSA-IgG in serum from 28 days post-transplant was significantly less in MMF-NP group compared to control and free MMF groups (control vs. free MMF vs. MMF-NP, 2914±156 vs. 2532±194 vs. 2043±79, n=4mice/group). (G) Elastica van Gieson stain of the allograft heart showed thinner intima in MMF-NP group compared to control and free MMF groups (control vs. free MMF vs. MMF-NP, 42.6±8.4 vs. 17.6±4.1 vs. 6.8±2.4, 2 random arteries from each mouse, n=4mice/group). (H) Gene expression of VCAM, ICAM and P-selectin in the allograft heart showed significantly less expression in MMF-NP group compared to control (control vs. free MMF vs. MMF-NP, 1.3±0.1 vs. 1.0±0.1 vs. 0.6±0.1 for VCAM, 0.9±0.02 vs. 0.8±0.1 vs. 0.7±0.09 for ICAM, 1.2±0.1 vs. 0.8±0.08 vs. 0.6±0.06 for P-selectin n=3mice/group). (J) HUVEC cells stimulated by TNFα showed high expression of VCAM, ICAM and P-selectin, which were suppressed by adding MMF-NP to a greater degree than by free MMF (control vs. free MMF vs. MMF-NP, 13.4±1.2 vs. 10.2±0.9 vs. 8.6±0.5 for VCAM, 27.4±3.0 vs. 15.9±2.3 vs. 7.1±1.2 for ICAM, 36.8±2.1 vs. 15.7±0.9 vs. 10.7±1.2 for P-selectin n=3mice/group).